Presented at 2008 Annual Hydrogen Conference and Hydrogen Expo USA
March 30 – April 3, Sacramento, CA

Analysis of Barriers for Mitigation of Unintended Releases of Hydrogen

W. Houf, R. Schefer, and G. Evans[1]

Abstract

Hydrogen jet flames resulting from ignition of unintended releases can be extensive in length and pose significant radiation and impingement hazards. Depending on the leak diameter and source pressure, the resulting consequence distances can be unacceptably large. One possible mitigation strategy to reduce exposure to jet flames is to incorporate barriers around hydrogen storage and delivery equipment. While reducing the extent of unacceptable consequences, the walls may introduce other hazards if not properly configured. An experimental and modeling program has been undertaken at Sandia National Laboratories to better characterize the effectiveness of barrier walls to reduce hazards. This paper describes the experimental and modeling program and presents results obtained for various barrier configurations. The experimental measurements include flame deflection using standard and infrared video and high speed movies (500 fps) to study initial flame propagation from the ignition source. Measurements of the ignition overpressure, wall deflection, radiative heat flux, and wall and gas temperature were also made at strategic locations. The modeling effort includes three-dimensional calculations of jet flame deflection by the barriers, computations of the thermal radiation field around barriers, predicted overpressure from ignition, and the computation of the concentration field from deflected unignited hydrogen releases. The various barrier designs are evaluated in terms of their mitigation effectiveness for the associated hazards present. The results show that barrier walls are effective at deflecting flames in a desired direction. While barrier walls can result in increased overpressures and radiative heat flux in the vicinity of the wall, they can also attenuate the effects of these hazards in surrounding areas if properly implemented.

[1] Sandia National Laboratory, Livermore, CA
Sandia is a multiprogram laboratory operated by Sandia Corporation,
a Lockheed Martin Company, for the United States Department of Energy's
National Nuclear Security Administration under Contract DE-AC04-94-AL85000.

1. Introduction

The development and commercial use of hydrogen will require safety guidelines for building vehicle fueling stations, storage facilities, and other infrastructure components. If the development of these safety guidelines is to be made on a scientific basis, then validated engineering models of unintended hydrogen releases are needed for scenario and risk analysis.

Hydrogen jet flames resulting from the ignition of unintended releases can be extensive in length and pose significant radiation and impingement hazards (Schefer et al., 2006, 2007). Depending on the leak diameter and source pressure the resulting consequence distances can be unacceptably large (Houf et al., 2007). One mitigation strategy for reducing the exposure to flames that can occur with unintended releases is to incorporate barriers around hydrogen storage equipment. The reasoning is that walls will reduce the extent of unacceptable consequences due to jet releases resulting from accidents involving high-pressure equipment. While reducing the jet extent, the walls may introduce other hazards if not properly configured. The goals of this work are to provide guidance on configuration and placement of these walls to minimize overall hazards and to provide quantitative information on barrier hazard distance reduction for use in safety guideline risk analysis.

While the use of barrier walls as a mitigation strategy is an important area of current research, the number of studies currently found in the literature is relatively sparse. Shirvill et al. (2006) investigated the explosion hazard consequences associated with high-pressure leaks from hydrogen vehicle refueling stations. The experiments used a dummy vehicle and dispenser units to represent refueling station congestion. Overpressures and radiative heat fluxes were measured in scenarios involving both the ignition of premixed hydrogen/air clouds and hydrogen jet releases. It was found that the overpressure produced during ignition depended on the ignition time relative to the time of release and whether the hydrogen was premixed or nonpremixed. The turbulence energy intensity also had a greater effect on explosiveness than the total amount of hydrogen leaked. The study concluded that it is not necessary to release a large volume of hydrogen to attain high overpressures and that the release of a smaller quantity of hydrogen with short ignition times in a region of high turbulence can result in significant overpressures.

Tanaka et al. (2005) carried out dispersion and explosion experiments in components associated with hydrogen refueling stations. Overpressures produced by sudden ignition of hydrogen released in a model hydrogen storage room and from a dispenser in a mock-up of a hydrogen vehicle fueling station were characterized. It was found that the overpressure produced in a confined enclosure varied significantly with hydrogen concentration. Also, the overpressure produced by ignition of a leak from the dispenser was found to be significantly affected by ignition time from the start of the release.

Tchouvelev et al. (2007) reported the results of a numerical modeling study to evaluate the effectiveness of small barriers at reducing clearance distances. The configuration consisted of a high-pressure hydrogen release impinging on a vertical 1 m by 1 m wall. Comparisons were made assuming both an ideal gas law and real gas properties using an Abel Nobel equation of state. Based on the predicted extent of the flammable gas concentration, the results confirmed that a small protective wall, or a barrier, can reduce the hydrogen concentration behind the wall, and thus the extent of the flammable gas envelope.

The purpose of the present study is to extend the available database on barrier walls as a hazard mitigation strategy and to provide technical data for risk-informed hydrogen codes and standards decisions regarding barrier wall design and implementation. The experimental effort is complemented by a parallel numerical modeling effort that considers the interaction of jet flames and unignited jets with barriers and the ignition overpressure. Results from the experiments are used to validate the Navier-Stokes simulations of barrier wall impingement and overpressure and provide a measure of confidence in the extension of the simulation capabilities to more complex barrier wall designs and release conditions. In the following sections the experimental and modeling results are presented for the barrier-wall configurations considered. The effectiveness of the barriers is evaluated in terms of: (a) the ability to deflect jet flames and protect downstream objects from flame impingement, (b) the reduction of exposure to jet flame thermal radiation, (c) the reduction of the extent of the flammable envelope from an unignited release, (d) the amount of ignition overpressure produced.

2. Jet Flame Barrier Wall Interaction Experiments

Four barrier tests were carried out with various wall heights and orientations using high-speed video and other suitable transducers to characterize the flame and wall interactions. The configurations of the four barrier wall tests are shown in Figure 1. A fifth test was also performed for a free hydrogen jet flame with no wall present to provide baseline data for evaluating the effectiveness of the barrier walls at hazard mitigation. All tests were carried out at the SRI International Corral Hollow test site in Tracy, CA. The data obtained during the tests provides a basis for direct evaluation of barrier effectiveness for flame hazards mitigation associated with accidental hydrogen leaks, as well as providing data for model validation.

The experimental setup for the first test (Test 1) is shown in Figure 1a and consisted of a horizontal hydrogen flame impinging on an approximately 2.4 m x 2.4 m (8 ft x 8 ft) cinderblock wall oriented vertically to the ground. The source of the hydrogen is a six-pack of high pressure storage cylinders. The jet issues through a 3.175 mm (1/8 in) diameter tube located 1.219 m (4 ft) from the barrier and directed toward its center, and provides up to a 400 second blow down period

before the cylinders are empty. The second test (Test 2) shown in Figure 1b was similar to the first, but the hydrogen jet and flame centerline were moved vertically upward so the height of the flame centerline equaled the wall height. The object of this test was to characterize the effect of wall height relative to the flame height. A question of particular interest was whether a flame that impinges closer to the top of the wall would be more likely to lead to a recirculation zone (and flame stabilization) behind the barrier wall. The third test (Test 3), shown in Figure 1c, consisted of a wall that was inclined to the vertical direction by 30 degrees. This configuration is of interest since it is based on National Fire Protection Association (NFPA) 68 guidelines (2006) for barrier walls (also referred to as blast deflector plates) where the recommended wall orientation is 30 to 45 degrees to the vertical. Under these conditions the wall acts as a flame deflector and should provide a smaller overpressure upon flame ignition. Test 4 involved measurements in a horizontal free jet flame 1.219 m (4 ft) off the ground with no wall present. This configuration was selected to provide a baseline data set for evaluating the effectiveness of the barrier wall at hazard mitigation. The jet diameter in this test was 3.175 mm, which was less than in previous free jet flame experiments (Schefer et al., 2006, 2007) but matches the jet diameter used in the other four tests with a wall present. The final configuration (Test 5) shown in Figure 1d consisted of three vertical walls, each approximately 2.4 m x 2.4 m square. In addition to the central cinderblock wall, two additional sidewalls were added with an angle between the walls of 135 degrees. This design is based on an International Fire Code (IFC) 2006 recommendation that a three-sided barrier is allowable as long as the connecting angle between the walls is not less than 135 degrees. Presumably three-sided configurations with connecting angles less than 135 degrees (for example 90 degree connecting walls) could produce potentially damaging overpressures due to the more restrictive confinement.

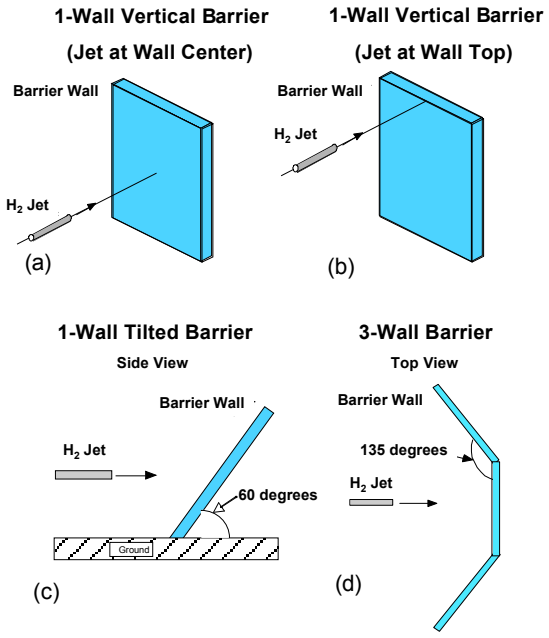

Figure 1. Schematics of barrier wall configurations for tests and calculations.

The barrier wall for Tests 1 and 2 was constructed of cinder blocks stacked in the vertical direction. Each cinder block measured 19.685 cm (7.75 in) thick by 19.05cm (7.50 in) tall by 39.37 cm (15.5 in) long and individual cinder blocks were cemented to adjacent blocks using grout. The wall was reinforced with vertical rebar rods extending the height of the wall and the hollow centers of the blocks (through which the rebar was placed) were filled with concrete. For all tests, the jet centerline was located 121.92 cm (48 in) above the ground and hence for Tests 1 and 5, the jet centerline actually intersected the vertical cinder block wall 3.175 cm (1.25 in) below the geometric center of the wall.

For the 1-wall tilted barrier in Test 3, a thinner wall material was used to facilitate the placement of the wall. The wall material for this test consisted of a steel panel that had a layer of backerboard on top. Backerboard is a fiberglass mesh-reinforced cement/concrete board approximately 2.286 cm (0.9 in) thick and is typically used as an underlayment for ceramic tile installed on walls, floors or countertops. In the 3-wall barrier Test 5, two backerboard walls were attached to the sides of the vertical cinder block wall to serve as the side walls. The angle between each side wall and the cinderblock wall was 135 degrees with the hydrogen jet approximately centered (see previous paragraph) on the center vertical cinder block wall.

A schematic of the flow delivery system used for the tests is shown in Figure 2. The hydrogen for the tests was provided by a "six-pack" of hydrogen cylinders, each individual cylinder with a volume of 43.8 liters (standard commercially-available size 1A). In previous tests (Schefer et al., 2006) using commercially-available "six packs", it was found that line restrictions in the manifold connecting the individual cylinders resulted in choked hydrogen flow and limited the available flow throughput. Thus the manifold lines leading from each cylinder were modified to prevent the flow from choking. Hydrogen needed to fill the custom "six-pack" before each test was provided by a cylinder farm of five commercial "six-packs". The modified hydrogen "six pack" source could be filled to approximately 13.79 MPa (2000 psi) immediately prior to each test.

The hydrogen was delivered to a stagnation chamber located just prior to the jet exit. The stagnation chamber was 29.2 cm in length with a 15.2 cm inside diameter and was sized to maintain an internal low flow Mach number (less than $1x10^{-3}$). At this Mach number, the measured pressure and temperature in the stagnation chamber are in excellent agreement with the true stagnation conditions. Both the stagnation chamber pressure and temperature histories were measured for the duration of each test. The temperature was measured with a type T thermocouple, while the pressure was measured using a piezoresistive pressure transducer. The jet exit conditions from the nozzle were calculated assuming isentropic expansion between the stagnation chamber and the horizontally-orientated 3.175 mm diameter jet exit where the flow was assumed to be choked. The jet diameter in the present experiments of 3.175 mm is smaller than the 5.08

mm (Schefer et al., 2007) and 7.94 mm (Schefer et al., 2006) jet diameters of the previous tests. This smaller diameter was selected to provide a longer blow down time and thus increase the test duration.

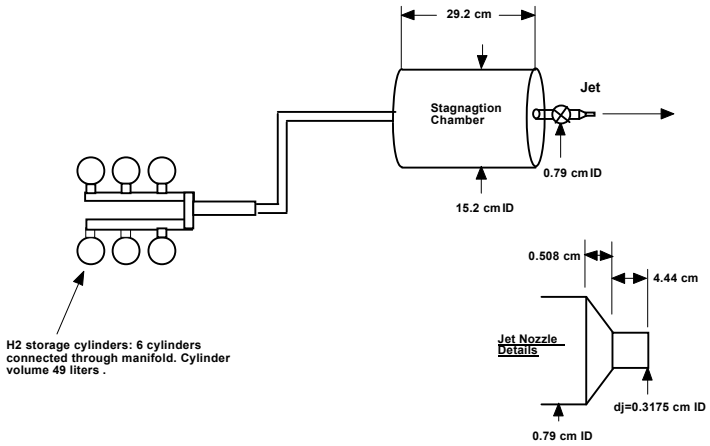

Figure 2. Schematic of experimental flow delivery system.

There was some variation in the initial storage pressure over the five tests carried out and the average initial pressure was measured to be 13.48±0.51 MPa (1956±75 psi). A pneumatic valve was placed between the stagnation chamber and the jet exit to prevent flow through the jet nozzle. The pneumatic valve was opened to start a test and allow hydrogen to be discharged through the jet exit. The time at which the valve reaches fully-opened is considered to be time zero, although all recording instrumentation begins about 5 seconds before time zero.

The hydrogen jet was ignited by a spark located 30.5 cm (12 in) in front of the wall and 12.7 cm (5 in) off the jet centerline at about the 7 o'clock position (when looking at the wall), or at an angle of 210 degrees from an upward vertical line. This location corresponds to the estimated position of the mixing layer adjacent to the hydrogen jet where the hydrogen has mixed with sufficient air to form a flammable mixture and the velocity is low enough to allow flame propagation upstream where a stable flame is formed. In all tests, successful ignition was achieved by a single spark and the spark ignition time was constant for all tests at 136.617 msec after the valve was fully opened.

The main purpose of the experimental tests was to characterize the effectiveness of the barrier wall configurations to deflect jet flames and to provide information about mitigating hazards such as thermal radiation and overpressure. Figure 3 shows the setup and instrumentation for the wall-centered jet flame test (Test 1). Both a visible wavelength standard video camera and an infrared video camera were located along the flame just prior to the wall to record the flame/wall interactions and the effectiveness of the wall at deflecting the flame. In addition, a high-speed Phantom camera (500-1000 frames per second) provided data on the

initial flame ignition process and subsequent propagation. Two heat flux gauges were located along the flame centerline prior to the wall to determine the radiative heat flux from the undisturbed portion of the free jet flame and an additional heat flux gage was located near the jet exit to characterize radiation received at the leak source (i.e. a storage tank, for example) from the deflected flame. Two heat flux gages were also placed behind the wall to determine the effectiveness of the wall at mitigating the flame radiation hazard. Also shown in Figure 3 are ten thermocouples located along the flame centerline, along the surface of the wall, and at a point just behind the wall.

Piezoelectric pressure transducers were also added to the experiments to measure the overpressures that occur due to ignition. The pressure transducers were placed along the ground with the sensor face typically located 6.35 cm (2.5 in) above the ground. The transducers were located before and after the wall to quantify the effectiveness of the wall at reducing the overpressures. In addition, a displacement sensor was placed on the back side of the wall at the center, approximately 30.48 cm (12 in) below the top of the wall. This was used to measure the deflection of the wall due to initial impact of the jet flow and the overpressure wave. The wall deflection was measured in Tests 1, 2 and 5 at the same location on the wall. This general experimental setup was used for each of the five tests, with some modifications as needed to accommodate the different wall configurations. For each test a weather station was used to record wind speed, wind direction, temperature, humidity and barometric pressure.

The standard visible and infrared video recordings from the tests were used to characterize the flame size and length, and the effectiveness of the barrier at deflecting the hot flame gases. Single frames taken from standard video recordings of the 4 barrier tests in the visible wavelength range are shown in Figure 4. The frames were taken at several seconds into the tests after transient effects due to initial hydrogen jet formation and flame ignition have diminished. Note that video recordings were also taken in one test consisting of a free jet with no wall present to provide a baseline data set for evaluating the effectiveness of the barrier wall at hazard mitigation. Shown in the frame for Test 1 (1-wall vertical barrier with jet at wall center in upper left frame) is the horizontal hydrogen flame impinging on the 2.4 m x 2.4 m cinderblock wall that is oriented vertically to the ground. The video image shows a 90 degree upward deflection of the flame, with no apparent flame stabilized behind the wall. The part of the flame that is deflected downward by the wall is seen to turn back toward the jet source as it impacts the ground. Depending on how close the wall is to the hydrogen source (i.e. storage tank, high pressure lines) this flame deflection toward the hydrogen source could result in an additional hazard due to heating of the source and potential equipment failures.

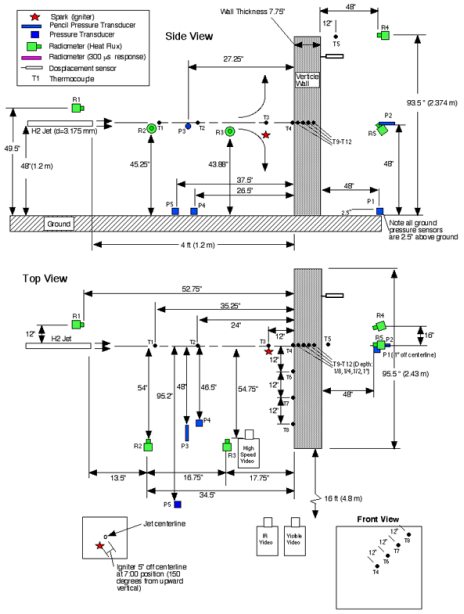

Figure 3. Schematic of instrumentation for Test 1, hydrogen jet centered on 2.4m x 2.4m cinderblock wall.

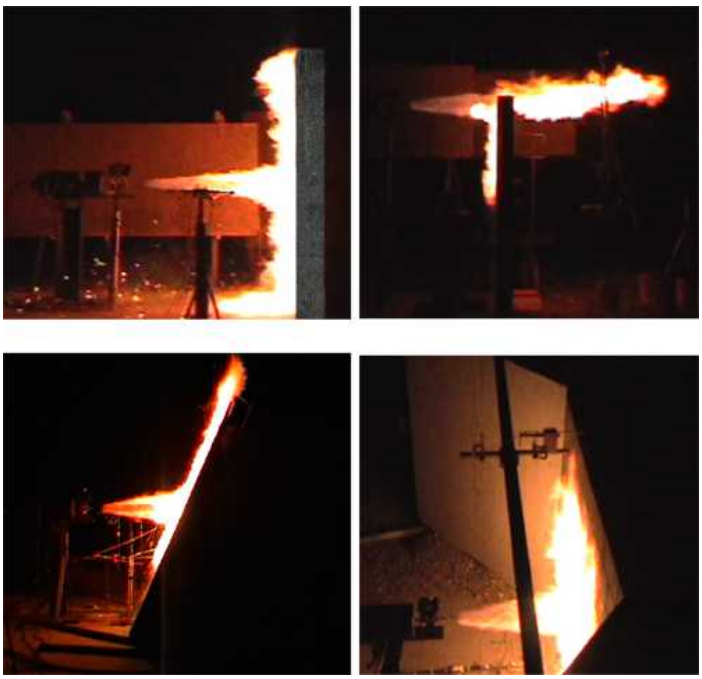

Figure 4. Standard video frames from barrier wall tests at SRI Corral Hollow Test site. Top left: Jet centered on 1-wall vertical barrier (Test 1); Top right: Jet located at top of 1-wall vertical barrier (Test 2); Bottom left: 1-wall barrier tilted at 30 degrees to vertical (Test 3); Bottom right: 3-wall vertical barrier with 135 degrees between walls (Test 5).

The single frame image for Test 2 (1-wall vertical barrier with jet at wall top in upper right frame of Fig. 4) shows the hydrogen jet and flame centerline raised vertically so that the height of the flame centerline equals the wall height. The

object of this test was to characterize the effect of wall height relative to the flame height. The lower half of the visible flame that intersects the wall is deflected downward along the front wall surface, while the top half of the flame passes over the top of the wall. While it was initially expected that a flame stabilization zone would be formed behind the wall, the video frame does not show this to be the case. Instead the flame appears to be only minimally deflected and extends nearly horizontally past the wall. No evidence was seen of any flame being entrained into the region behind the wall and below the jet, and the corresponding infrared images (not shown) also confirm the lack of any flame in this region.

The lower left frame of Figure 4 shows the flame interaction with a 1-wall barrier that was tilted to the vertical direction by 30 degrees (Test 3). Under these conditions the wall should act as a flame deflector and provide a smaller overpressure upon flame ignition. Similar to the 1-wall vertical barrier configuration, part of the flame is deflected upward along the surface of the wall and the remainder is deflected downward. It should be noted that the downward-deflected flame segment only extends about half way down the wall surface and does not reach the ground as was seen with the 1-wall vertical barrier (top left frame). This configuration thus might more effectively reduce the potential hazard associated with heating of the hydrogen source as noted above. The part of the flame deflected up along the wall surface continues past the top edge of the wall and maintains the same angle as the wall surface, again showing no flame entering the region behind the wall.

The visible flame image for Test 5, seen in the lower right frame of Figure 4, is for the 3-wall barrier with an angle of 135 degrees between each of the vertical walls. The videos cameras were located higher off the ground and the view of the cameras is over one of the sidewalls looking downward at an angle to the flame impingement point. The flame is again deflected outward from the wall impact point by the center cinderblock wall. However, the visible, luminous flame does not appear to extend past the center wall to the sidewalls, nor does the flame appear to extend above the top of the center wall as is seen in Test 1 for the jet at wall center configuration. Since in both tests the jet axis is 1.2 m above the ground and the flame impacts the midpoint of the center wall, this difference is somewhat surprising. The corresponding infrared image confirms the lack of flame gases above the top edge of the wall, implying that the gases have cooled sufficiently in the 3-wall barrier Test 5 so as to not be observable in either the visible or infrared videos.

Pressure measurements obtained during each of the five tests are summarized in Figure 5. In the top graph, the maximum overpressures measured by transducer P4, located approximately 0.6 m in front of the wall (see Figure 3), are shown. It can be seen that the maximum overpressure of 6.89 kPa (1 psi) is measured in the 1-wall vertical barrier test with the jet centered on the wall. Pressures in both the 1-wall tilted barrier and the 3-wall barrier are lower but still exceed 4.14 kPa (0.6 psi). For reference, pressures generated in the free jet with no wall present are

about 2.76 kPa (0.4 psi). The case with the 1-wall vertical barrier with the jet raised to the height of the wall is very comparable to the free jet. This latter observation is likely due to the fact that with the jet located at the top of the wall, there is little confinement effect imposed by the wall on the expanding combusted gases. The measured overpressure levels are well below the overpressures associated with personal injury from eardrum rupture (appox. 35 kPa (5 psi)) (AICHE, 1994). The lower graph in Figure 5 shows the ratio of the maximum overpressure after the wall, P1, to that measured in front of the wall, P4. The value of P1/P4 is unity for the free jet since no wall is present. The 1-wall vertical barrier configuration with the jet located at the top of the wall is somewhat effective at reducing the pressure behind the wall, reducing the overpressure ratio by about 20%. The 1-wall tilted barrier, 1-wall vertical barrier with centered jet and 3-wall barrier all reduce P1/P4 by greater than a factor of five, with the 3-wall barrier reducing P1/P4 by nearly an order of magnitude. It should be noted that the maximum pressure on the front and back side of the wall may not be located exactly at the positions of P4 and P1.

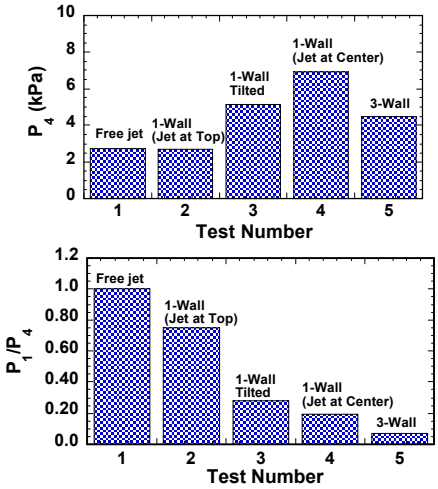

Figure 5. Overpressures measured in a free jet and each of four barrier wall configurations. Top graph: Maximum overpressure measured prior to wall; Lower graph: Ratio of maximum overpressure measured after wall to overpressure behind wall.

The radiative heat fluxes measured in the various test configurations are summarized in Figure 6. The results shown correspond to a time of 25 seconds into the test when the radiative heat flux is near the maximum. Figure 6 shows that the highest radiant heat fluxes measured by R1 near the jet exit are in the jet centered at wall configuration. Values for the jet at wall top, the inclined wall, and the three-sided wall are comparable, while the free jet heat fluxes are the lowest. Shown in Figure 6 are the values of heat flux measured at 25 seconds by R4 located behind the wall and looking at an angle toward the top of the wall. A comparison of this measurement with the heat flux measured in front of the wall provides a measure of the effectiveness of the barrier wall to mitigate the hazard associated with radiative heat flux. It can be seen that the jet at wall top configuration of Test 2 effectively reduces the heat flux by about a factor of 2.5

(R1 and R4 are 10 kW/m^2 and 3.8 kW/m^2, respectively). The inclined wall and jet at wall center configurations reduce the heat flux by factors of 17 and 40, respectively, while the reduction with the three-sided wall is nearly a factor of 130.

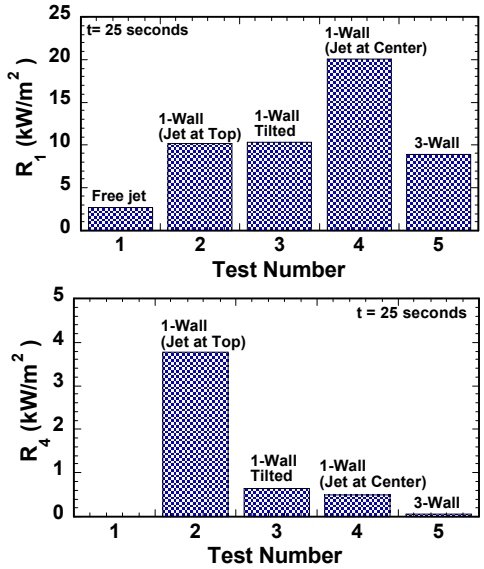

Figure 6. Maximum radiative heat flux at 25 seconds into test measured in a free jet and each of four barrier wall configurations. Top graph; Heat flux measured at jet origin; Lower graph: Heat flux measured behind wall.

3. Jet-Barrier Wall Interaction Modeling

The purpose of the barrier modeling study is to assess the effectiveness of various barrier designs in terms of: (1) deflecting the jet flames, (2) reducing the extent of the flammable cloud resulting from an unignited release, (3) reducing the magnitude of the radiative heat flux produced by the jet flame from an ignited release (4) and minimizing the amount of ignition overpressure produced from the barrier confinement. Calculations of unignited and ignited turbulent jets were performed with the Sandia developed code, FUEGO, designed to simulate turbulent, reacting flow and heat transfer (Moen et al., 2002) on massively parallel computers, with a primary focus on heat transfer to objects in pool fires. The code has recently been adapted for compressible flow and hydrogen combustion. The discretization scheme used in FUEGO is based on the control volume finite element method (Schneider, 1988), where the partial differential equations for conservation of mass, momentum, and energy are integrated over unstructured control volumes. A two equation (k-ε) turbulence model is applied to close the Favre averaged equations and the results presented here have been obtained using a slightly modified RNG k-ε model (Papageorgakis, 1999). Transport equations are solved for the mass fractions of each chemical species, except for the dominant species (N_2 in the present simulations) which is computed by constraining the sum of the species mass fractions to equal one. For compressible flow, the ideal gas equation of state is used to relate the density and

pressure of the gas mixture. Combustion of hydrogen is modeled with the EDC model of Magnussen (1989), a one-step irreversible conversion of H_2 and O_2 to H_2O where the time scale for chemical reaction is based on the integral turbulent time scale as given by k/ε. For the calculations reported here, the first order upwind scheme was used for the convective terms. Although the code solves the conservation equations in a time-dependent manner the results presented here are for steady conditions.

Radiative heat loss from hydrogen flames is important in determining the flame temperature. The radiation transport was computed with the Sandia developed finite element code SYRINX (Burns, 1999), a discrete ordinates, participating media radiation heat transfer code that is coupled to FUEGO. The directional integration of the radiative transfer equation was carried out using the TN quadrature method (Thurgood et al., 1995). The radiative energy transfer calculated in SYRINX is coupled to FUEGO through a radiative source term in the energy equation and the radiative transport is assumed to be gray (single absorption coefficient). The single absorption coefficient was determined using the model of Leckner (1972) which accounts for the presence of CO_2 and water vapor in addition to soot. Because there is no soot or CO_2 in a hydrogen flame only the absorption of radiation from the spectral bands of water vapor were included from the Leckner model. Initial calculations showed an over prediction of the radiative heat flux as compared to the free jet flame radiometer measurements made as part of Test 4 (see section above). Two parameters in the absorption coefficient model, a length scale and a scale factor, were adjusted to obtain agreement with the data for the free hydrogen jet flame. These parameters have not been adjusted subsequently in the prediction of radiative heat transfer in the simulations of hydrogen jet flames against barriers.

The hydrogen releases modeled are the barrier wall experiments discussed in Section 2.0, where high-pressure sources (initial stagnation pressures of approximately 13.79MPa (2000psi)) result in momentum-dominated underexpanded jet flows. The flows are choked at the jet orifice and expand supersonically into ambient air for most of the blowdown event. The blowdowns last several minutes, during which the stagnation pressure and jet flame length gradually decrease and at any particular time during the blowdown (beyond the initial startup and ignition of the jet) the flow field and heat and mass transfer (with the exception of heat conduction into the barrier) can be considered quasi-steady.

From a CFD perspective the concept of using a pseudo-diameter for the jet opening is attractive if the velocity at the pseudo-diameter (e.g. Birch et al., 1984) is subsonic. In this case, the boundary condition for a turbulent jet calculation avoids the complex supersonic expansion between the sonic condition at the jet opening and the eventual subsonic flow downstream in the ambient. The Mach disk analysis of Winters et al. (2006) results in a subsonic condition at the downstream side of the Mach disk. In the Mach disk analysis an isentropic

expansion is assumed between stagnation conditions upstream of the jet opening and the sonic condition at the jet exit. An isentropic expansion is also assumed from the jet exit to just upstream of the Mach disk where normal shock relations as given in Shapiro (1953) are applied to give conditions downstream of the Mach disk. In the present analysis all the gas flowing through the jet opening is assumed to pass through the Mach disk. The computed Mach disk diameter becomes the pseudo-diameter for the jet simulation and the post shock velocity and temperature become the jet exit conditions. Hence, the Mach disk model (Winters et al., 2006) provides a subsonic jet inflow boundary condition for the FUEGO simulations discussed below.

A validation study of the ability of the model to predict the velocity and concentration decay along the centerline of unignited hydrogen free jets and the centerline temperature profile for laboratory-scale and large-scale hydrogen jet flames was reported in Houf et al. (2007). Results for the concentration decay of hydrogen (either mass or mole fraction) using the RNG k-ε turbulence model show decay constants ranging from 5.0 to 5.5 which are in good agreement with experimental data. Figure 7 shows reasonably good agreement between the calculated (curves shown for jet inlet turbulence intensities of 2% and 10% and using the standard and the RNG k-ε turbulence models) and measured centerline temperature distributions for the hydrogen air jet flame of Barlow, 1994.

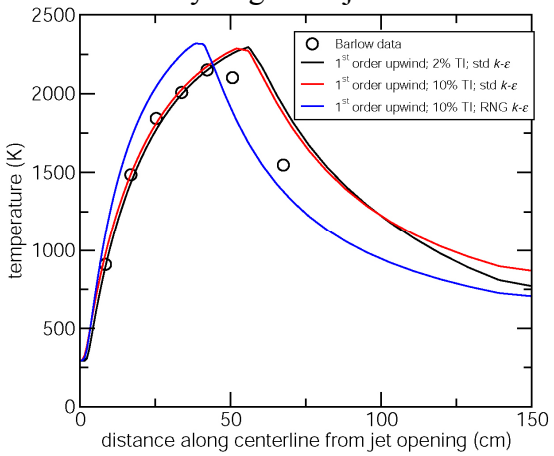

Figure 7. Jet centerline temperature distributions for incompressible, turbulent hydrogen air jet flame (flame A of Barlow et al., 1994); Re_d=1.0x10^4.

Simulations have been performed for both unignited and ignited releases for the jet barrier impingement experimental geometries described in Section 2.0. In both unignited and ignited simulations the jet exit conditions were calculated from the measured stagnation chamber conditions a short time after the start of the blowdown (approx. 6.3 sec) when the flow or jet flame was well established. The mesh distributions for both the ignited and unignited barrier simulations were identical, except that the mesh was doubled for the ignited case because no symmetry boundary condition was available for the radiation transport calculation. Except as noted below, the three-dimensional computational domain

consisted of a 625 cm by 914 cm by 1360 cm rectangular domain in the (x,y,z) coordinate directions with the jet inflow boundary centered at the origin and the jet aligned in the +z direction. The jet is horizontal and located 121.9 cm (4 ft) above the ground (at y=-121.9 cm). For the unignited calculations the y-z plane at x=0 is a vertical symmetry plane passing through the centerline of the jet. Figure 8 shows the mesh distribution used for the simulation of Test 1 where the jet impinges on a vertical barrier. In all barrier simulations the jet origin was located 121.9 cm upstream of the barrier (the upstream surface of a vertical barrier is at z=121.9 cm). Approximately 550,000 and 750,000 computational cells were used in the unignited simulations of a free jet and a jet against a barrier, respectively. Twice as many computational cells were used for the corresponding ignited jet calculations without a symmetry plane. The turbulent Prandtl and Schmidt numbers used in the calculations were 0.9.

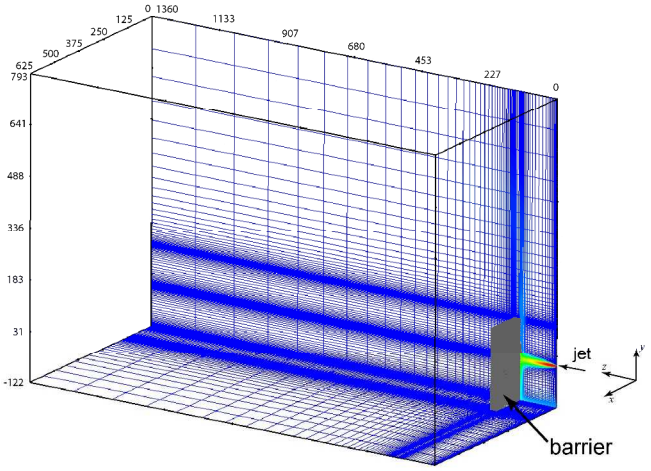

Figure 8. Half of the computational domain showing mesh distribution and jet and barrier locations for Test 1 (1-wall vertical barrier jet at center) configuration.

The jet flame barrier wall interaction experiments described in Section 2.0 start from approximately the same initial pressure and temperature with similar blowdown histories in which the hydrogen jet issues from a 3.175 mm diameter tube. For all simulations the stagnation pressure and temperature used to determine the inflow boundary conditions with the Mach disk analysis were 10.327 MPa (1497.8 psia) and 278.14K, respectively (this condition corresponded to a time of 6.35 seconds into the blowdown in Test 1, where the jet flame was directed toward the center of a vertical 8 ft x 8 ft barrier). For these conditions, the Mach disk calculation for pure hydrogen yielded a pseudo-diameter of 4.05 cm, with an inflow velocity and temperature of 498.7 m/sec and 274.94K, respectively. Inflow turbulence quantities were 20% turbulence intensity with a turbulence length scale of 4.05 cm. Boundary conditions for the ground plane and the barrier were no-slip, adiabatic, and reflective. All other boundaries except the jet inflow were assigned open boundary conditions with a total pressure of 1 atmosphere (101.33kPa), a temperature of 298K, O_2 and N_2 mole fractions of 0.21

and 0.79, respectively and negligible turbulence (k=1.0x10^{-4} cm^2/sec^2, ε=1.0x10^{-3} cm^2/sec^3) with a radiation transmittance of 100%.

3.1 Jet Flame Barrier Deflection and Radiation Simulations

Figure 9 shows Fuego jet flame simulations of the 4 barrier interaction experiments discussed in Section 2.0. These simulations were made prior to performing the tests and were used to help guide the proper placement of sensors for the experiments. Comparisons of the video clips from the tests (see Fig. 4) with the temperature color contour plots (Fig. 9) indicate that the model correctly predicts the deflected jet flames observed in the experiments. Figure 9b shows the simulation for Test 2 (1-wall barrier jet at top) and indicates that the lower half of the flame intersects the wall and is deflected downward along the front of the barrier, while the top half of the flame passes over the top of the wall. While it was initially expected that a flame stabilization zone would be formed behind the wall, this pre-test simulation showed no evidence of flame being entrained into the region behind the wall and allowed proper placement of sensors and cameras for the experiment. Visible as well as infrared images and thermocouple temperature measurements (not shown) from the test confirm the lack of any flame in the region behind the wall and below the jet.

Figure 10 shows computed isosurfaces of radiative heat flux of 4.7 kW/m^2 for a free hydrogen jet flame (Fig. 10a) of Test 4 and a hydrogen jet flame impinging on a vertical barrier (Fig. 10b) of Test 1. The heat flux level of 4.7 kW/m^2 is the allowable exposure for employees for a maximum of 3 minutes (International Fire Code, 2006). The reduction in horizontal extent of the radiation field with a barrier is clearly seen in Fig. 10c where side views of the isosurfaces from the two cases are superimposed. Figure 10 also shows that the barrier causes the vertical extent of the 4.7 kW/m2 heat flux level to be slightly greater (upstream of the barrier) than for the case of a free jet flame.

Predicted radiative heat fluxes were validated by comparing to data from the horizontal free jet flame experiment of Test 4. As previously mentioned the absorption coefficient model in SYRINX was scaled to achieve good agreement with the experimental data for the radiative heat flux for this free jet flame experiment (Test 4). The scaled absorption model was then used to perform radiation calculations for the jet flame on barrier configurations. Comparisons between the model and Test 4 data and the predicted effect of a 1-wall vertical barrier in reducing the radiation downstream of the barrier are shown in Fig. 11. The radiative heat flux is computed at a radial position of 137.6 cm from the jet centerline where the radiometers were located. Figure 11 also shows the predicted radiative heat flux (dashed curve) for the case of the jet flame centered on a 1-wall vertical barrier (Test 1) where the heat flux is plotted at the same radial distance from the jet centerline (137.6 cm). The predicted radiative heat flux for the case with the vertical barrier is larger than the free jet radiative heat

flux upstream of the barrier and smaller than the free jet result downstream of the barrier. The sharp drop and increase in the predicted heat flux just upstream of the barrier is due to the lateral spread of the jet flame beyond 137.6 cm from the jet centerline as the jet flame turns from an axial jet into an axisymmetric laterally spreading jet at the barrier (see Fig. 10b).

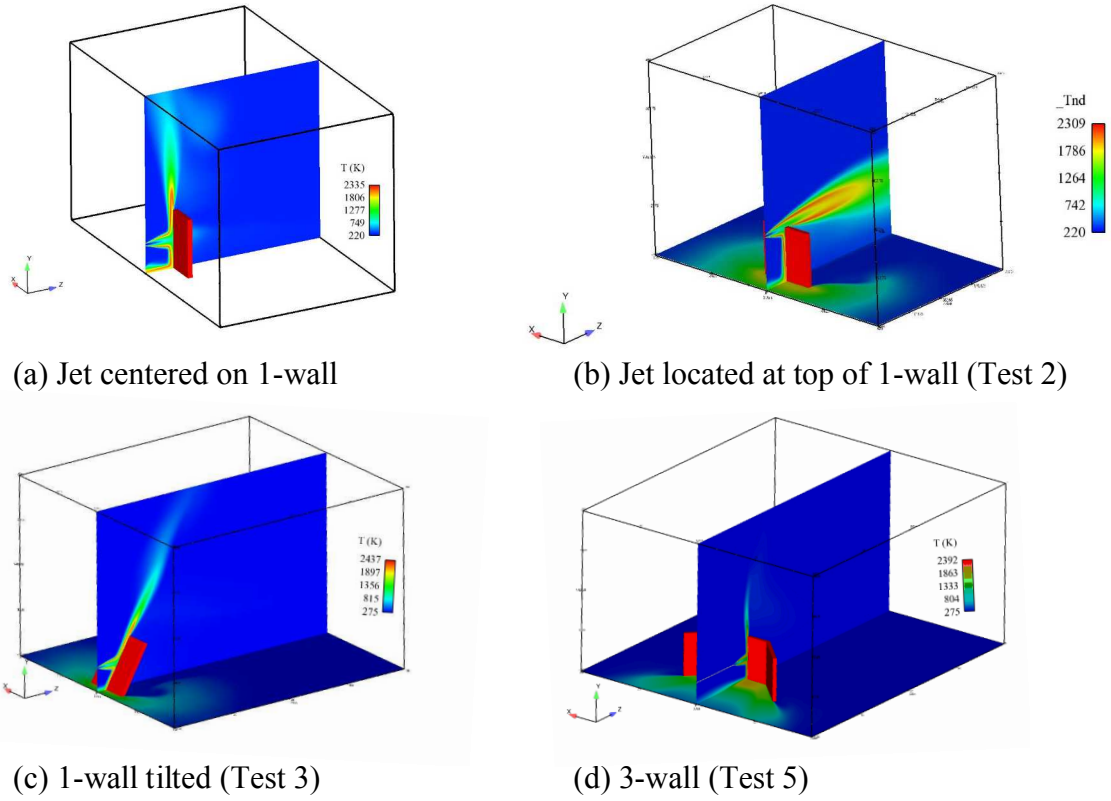

(a) Jet centered on 1-wall

(b) Jet located at top of 1-wall (Test 2)

(c) 1-wall tilted (Test 3)

(d) 3-wall (Test 5)

Figure 9. Hydrogen jet flame on barrier simulations for the 4 different experimental test configurations.

Predictions of the isosurfaces for a radiative heat flux level of 4.7 kW/m^2 for the 1-wall tilted barrier and the 3-wall barrier are compared with results for the 1-wall vertical barrier in Fig. 12. For the 3-wall barrier calculation the computational domain was extended upstream of the jet release by 330 cm and 1.96x10^6 computational cells were used for the simulation. In Fig. 12a the 4.7 kW/m^2 radiation heat flux isosurface extends farther in the downstream and vertical directions for the tilted barrier compared with the vertical barrier result. In Fig. 12b the 4.7 kW/m^2 radiation heat flux isosurface has a larger vertical extent for the 3-wall barrier than for the 1-wall vertical barrier while the horizontal extent is approximately the same for the two cases.

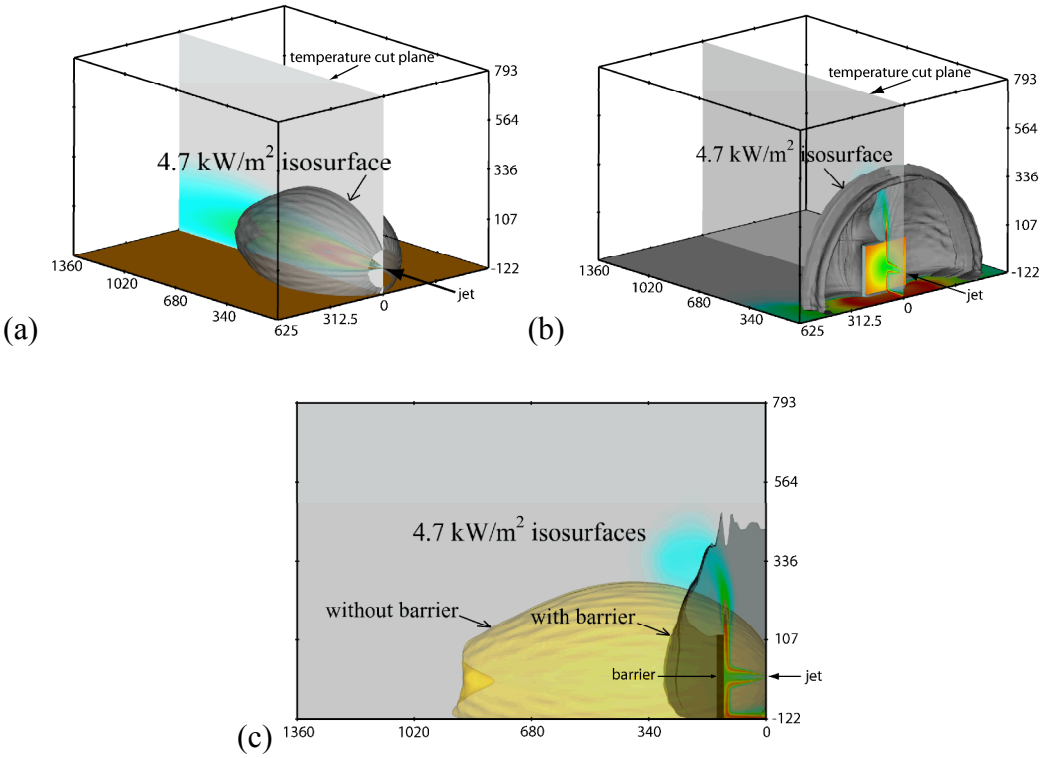

Figure 10. Calculated isosurfaces for radiative heat flux of 4.7 kW/m^2 from hydrogen jet flames; (a) free jet flame with ground plane; (b) jet flame directed toward center of 1-wall vertical barrier; (c) side view of isosurfaces shown in (a) and (b), comparing horizontal and vertical extent of radiation field without and with a barrier; jet flow is from right to left with distances in centimeters.

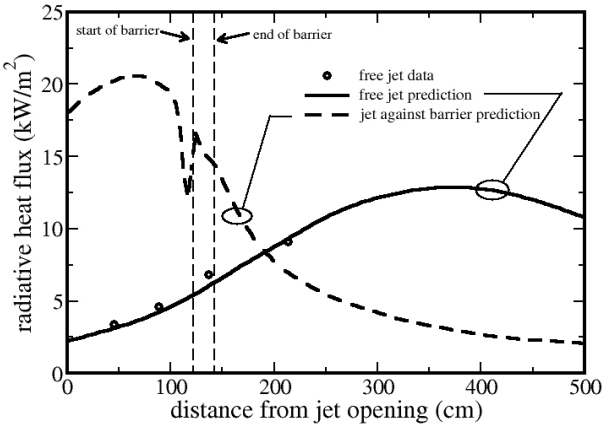

Figure 11. Comparison of measured and predicted (solid line) radiative heat flux from a horizontal free hydrogen jet flame along a line parallel to the jet. Also shown is the predicted heat flux (dashed line) when the jet flame is directed toward the center of a 2.4 m x 2.4 m (8 ft x 8 ft) vertical barrier. Predictions and data are for a lateral distance of 137.6 cm from the jet centerline. Predictions use an absorption coefficient scale factor and length scale of 0.2 and 100 cm, respectively and the TN quadrature with 12 ordinates.

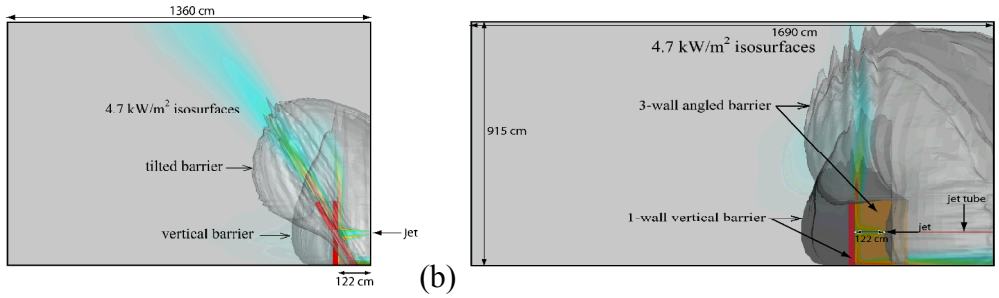

Figure 12. Comparisons of side views of calculated isosurfaces of radiative heat flux levels of 4.7kW/m^2 from hydrogen jet flames directed at barriers showing horizontal and vertical extent of radiation; (a) 1-wall tilted barrier and 1-wall vertical barrier superimposed; (b) 3-wall barrier and 1-wall vertical barrier superimposed; jet flow is from right to left.

Table I. Model results comparing maximum axial and lateral distances for several levels of radiative heat flux from a free hydrogen jet flame and a hydrogen jet flame directed toward the centers of the different barrier configurations.

Radiative Heat Flux (kW/m^2)	Geometry	Axial Extent (m)	Lateral Extent (m)
1.5	free jet	>13.5	5.7 @ z=3.9
1.5	1-wall vertical barrier	4.9	>6.3 @ z<3.7
1.5	1-wall tilted barrier	9.1	>6.3 @ z<6.5
1.5	3-wall barrier	5	>7.6 @ z<1.9
4.7	free jet	8.8	2.8 @ z=3.8
4.7	1-wall vertical barrier	3. @ x=2.3	4.9 @ z=1.1
4.7	1-wall tilted barrier	4.5 @ y=2.2	4.2 @ z=2.4
4.7	3-wall barrier	2.9 @ y=3.8	6.6 @ z=-2.6
20	free jet	5.2	1. @ z=3.5
20	1-wall vertical barrier	1.5 @ x=1.7	2.4 @ z=1.2
20	1-wall tilted barrier	2.1 @ y=2	1.6 @ z=1.6
20	3-wall barrier	1.5 @ y=2	4.2 @ z=-2.1
25	free jet	4.7	0.8 @ z=3.5
25	1-wall vertical barrier	1.4 @ x=1.6	2. @ z=1.2
25	1-wall tilted barrier	1.6 @ y=1.1	0.86 @ z=1.6
25	3-wall barrier	1.3 @ y=1.8	3.9 @ z=-1.6

Model results for the maximum axial and lateral distances to several radiative heat flux levels for the free hydrogen jet flame (Test 4) and the 3 barrier configurations (1-wall vertical, 1-wall tilted, and 3-wall) are compared in Table I. Results are shown for heat flux levels of 1.5 kW/m^2, 4.7 kW/m^2, 20 kW/m^2, and 25kW/m^2.

These values correspond (in order of increasing magnitude) to values listed in the International Fire Code (2006) for exposure at property line, exposure for employees for a maximum of 3 minutes, exposure for combustible equipment, and exposure for non-combustible equipment. For all heat flux levels the barriers reduce the axial distance to the specified radiation level significantly as compared to a free jet flame and only increase the lateral distance slightly. When comparing the various barrier configurations, the axial distance is greatest for the 1-wall tilted barrier and the lateral distance is largest for the 3-wall barrier.

3.2 Unignited Jet Concentration Envelope Simulations

The purpose of this work is to address how barriers can reduce flammability envelope hazard distances for unignited releases of hydrogen. The same barrier (1-wall vertical, 1-wall tilted, 3-wall) and free jet configurations studied for the ignited jet barrier interaction simulations discussed in Section 3.1 were simulated for unignited conditions to calculate concentration envelopes. The jet exit boundary conditions used for the ignited simulations were again used for the unignited simulations and correspond to exit conditions (at approx. 6.3 sec) for the experimental tests discussed in Section 2.0.

The generally accepted value for the upward-propagating lower flammability limit of hydrogen in air is 4% mole fraction, but experimental data in the literature indicate that the limit may be as high as 7.2% mole fraction for horizontal-prorogating flames and 9.5% mole fraction for downward-propagating flames (Zebatakis, 1965; Coward and Jones, 1952). Figure 13 shows the unignited isosurfaces for hydrogen mole fractions of 4% and 8% for a horizontal jet impinging on the center of the 1-wall 2.4 m x 2.4 m (8 ft x 8 ft) tilted barrier (only half of the domain was computed and the results have been reflected about the *y*-*z* symmetry plane for visualization). The hydrogen jet is located 1.219 m (ft) above the ground and 1.219 m (4 ft) from the center of the wall. The 8% mole fraction surface extends to a maximum of 2.7 meters in the axial direction from the jet exit while the 4% mole fraction surface extends 4.4 meters. A calculation of the horizontal extent of the concentration decay for a free jet using the jet concentration scaling law (Houf and Schefer, 2007) with the Mach disk pseudo-diameter indicates that the 8% mole fraction surface would extend 10.4 m from the jet exit while the 4% mole fraction surface would extend approximately 20.8 m.

Figure 14 shows the 4% and 8% hydrogen mole fraction isosurfaces for the unignited jet impinging on the 1-wall vertical and 3-wall (135 degrees between walls) barrier configurations. In both cases the jet is directed at the center of 2.4m x 2.4m (8 ft x 8 ft) central cinderblock wall which is 20.32 cm (8 in) thick. In both the simulations the jet release is located 1.219 m (4 ft) away from the central wall. Figure 14 shows that the effect of these two barrier configurations is to confine the hydrogen to a region essentially upstream of the barriers, greatly

reducing the downstream (axial) extent of the unignited release as compared to the case with no barrier or the 1-wall tilted barrier.

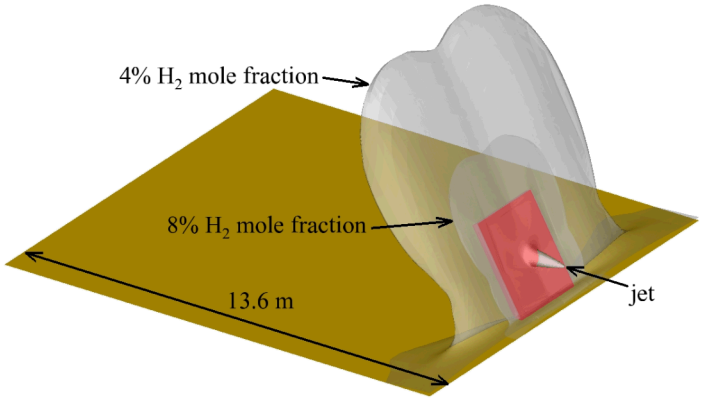

Figure 13. Calculated isosurfaces of 4% and 8% hydrogen mole fraction for a horizontal jet impinging on the 1-wall 2.4 m x 2.4 m (8 ft x 8 ft) tilted barrier. The jet release location is 1.219 m above the ground with the flow from right to left.

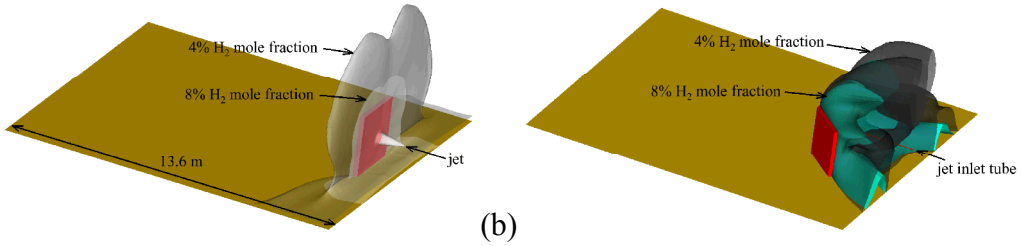

(a) (b)

Figure 14. Calculated isosurfaces of 4% and 8% hydrogen mole fraction for unignited horizontal jets impinging on barriers with jet flow from right to left. (a) 1-wall 2.4 m x 2.4 m (8 ft x 8 ft) vertical barrier; (b) 3-wall barrier with 135 degrees between each 2.4 m x 2.4 m (8 ft x 8 ft) wall.

3.3 Ignition Overpressure Simulations of Jet Barrier Impingement Releases

The purpose of this work is to investigate the amount of overpressure produced from the ignition of an impinging jet release into a barrier and how that pressure is attenuated by the barrier. Simulations of jet releases into the 3 barrier configurations (1-wall vertical, 1-wall tilted, and 3-wall) and the computation of the overpressure from ignition for various release times were performed using the FLACS (2003) Navier-Stokes code. To begin the simulations, FLACS was used to model the overpressure measured from the 1-wall vertical barrier experiment (Test 1) discussed in Section 2.0. The Test 1 geometry was modeled as a single 2.4 m x 2.4 m vertical wall that was 20.32 cm thick. The 3.175 mm diameter jet orifice was located a distance of 1.219 m away from the wall and 1.219 m above the ground with the jet centerline aligned with the center of the wall. The FLACS Jet Utility program was used to calculate the pseudo-diameter of the jet exit and

the subsonic jet exit conditions for use as jet exit boundary conditions in the model. The pressure and temperature used to calculate the jet exit conditions were the pressure and temperature measured in the stagnation chamber of the experiment (Test 1) at the moment when the jet exit valve was fully opened (appox. 12.28MPa, 289K). The unignited jet simulation was allowed to run for 136.617 msec prior to initiating ignition in the simulation. The ignition source was located in the model at 30.5 cm (12 in) in front of the wall and 12.7 cm (5 in) off the jet centerline at the 7 o'clock position (when looking at the wall) as in the Test 1 experiment. Pressure versus time monitors were placed in the model at the same locations where pressure transducers were placed in the Test 1 experiment (see Fig. 3). Figure 15 shows a comparison of the predicted and simulated overpressure pulse at pressure transducer P4 located on the front side of the wall (jet side) and pressure transducer P1 located on the back side (downstream) of the wall (see Fig. 3). Pressure transducer P4 is located 67.31cm (26.5 in) from the front wall and 118.1 cm (46.5 in) off the centerline of the wall at a distance of 6.35cm (2.5 in) off the ground. Pressure transducer P1 is located at a distance of 121.92cm behind the back side of the wall, 2.54 cm (1 in) off the centerline of the wall and 6.35 cm (2.5 in) off the ground. Figure 15 shows that the predicted peak overpressure on the front side and back side (downstream) of the barrier is approximately 19% greater than the measured overpressure.

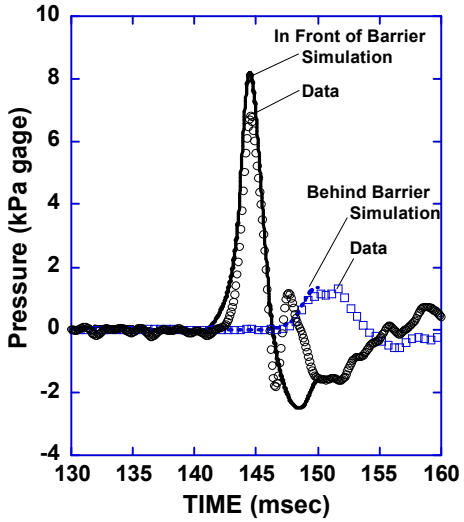

Figure 15. Comparison of simulation of overpressure from ignition of impinging hydrogen jet on the center of a 1-wall vertical barrier with pressure transducer measurements from experimental Test 1 (ignition occurs at 136.617msec).

Simulations were also performed for larger release times prior to ignition for both the 1-wall vertical barrier configuration of Test 1 and the 3-wall barrier configuration of Test 5. The ignition position was kept the same for all simulations and corresponded to the ignition location for the experiments. Figure 16 shows the peak overpressure computed for simulations of the 1-wall vertical barrier and 3-wall barrier configurations as a function of the release time before ignition. The peak overpressure occurs near the front face of the central wall in both cases. Also shown on the plot is the temporal variation of the equivalent

stoichiometric cloud (FLACS, 2003) based on the volume of the unignited hydrogen/air cloud that accumulates around the barrier during the release. Simulated peak overpressures on the front side of the barrier are approximately 39kPa for the 1-wall vertical barrier (Test 1) as compared to approximately 41kPa for the 3-wall barrier (Test 5) configuration. The measured stagnation chamber pressure was approximately 12.28 MPa (1782.25 psig) for Test 1 and approximately 12.84 MPa (1862.5 psig) for Test 5 and these values were used in the respective simulations.

Figure 17 shows a comparison of the simulation of the maximum overpressure after ignition for the 1-wall vertical barrier (Test 1 configuration and conditions) as compared to the 3-wall barrier (Test 5 configuration and conditions) for a 1 second release prior to ignition. The central wall is a 2.4 m x 2.4 m vertical wall that is 20.32 cm thick for both simulations. For the 3-wall simulation the outer walls are also 2.4m x 2.4m vertical walls (2.28 cm (0.9 inches) thick) that connect to the central wall at an angle of 135 degrees. Peak computed overpressure on the back side (downstream) of the 1-wall vertical barrier is less than approximately 5.5 kPa while the peak overpressure on the front side is 38.1 kPa. The peak computed overpressure on the back side of the 3-wall barrier is less than approximately 3kPa while the peak overpressure on the front side is 39.7 kPa.

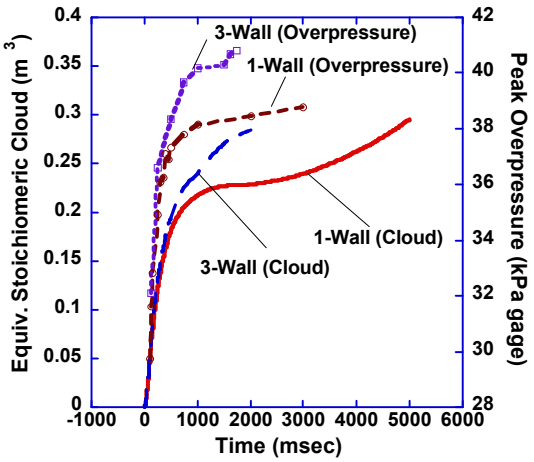

Figure 16. Comparison of peak overpressure and equivalent stoichiometric cloud for 1-wall vertical barrier (Test 1) and 3-wall barrier (Test 5).

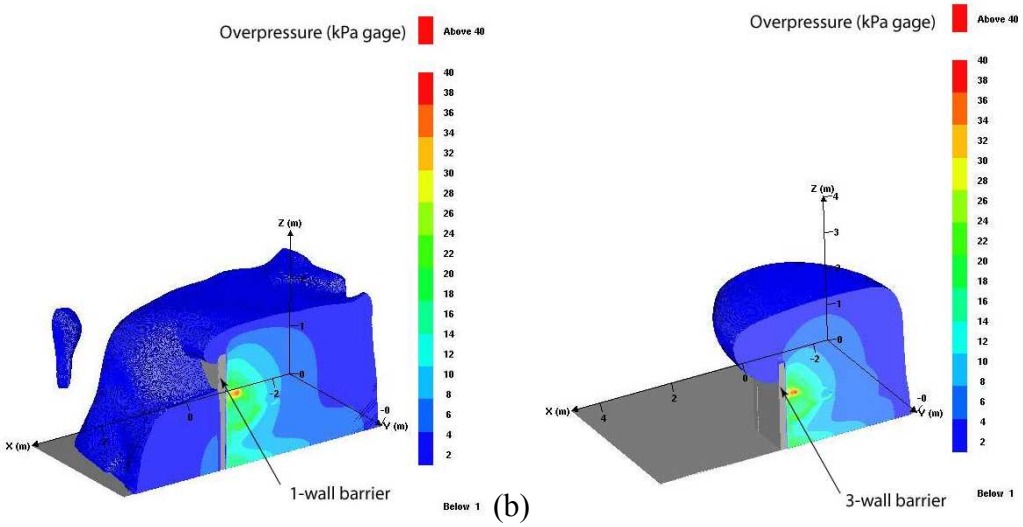

(a) (b)

Figure 17. Comparison of maximum overpressure for (a) 1-wall vertical barrier (Test 1) and (b) 3-wall barrier with 135 degrees between each wall (Test 5) for ignition after 1 second from the beginning of the release (1/2 domain shown). Pressure scales are identical on both plots and distances are shown in meters. The outer boundary of the isosurface is 1kPa in both plots and the jet flow is from right to left with ignition on the front side (right) of the barrier.

4. Summary and Conclusion

A combined experimental and simulation study has been performed to assess the effectiveness of barriers to reduce the hazard from unintended releases of hydrogen. For the conditions investigated 13.79MPa (2000psi) source pressure and 3.175mm (1/8in) diameter round leak the barrier configurations studied were found to (1) reduce horizontal jet flame impingement hazard by deflecting the jet flame, (2) reduce radiation hazard distances for horizontal jet flames, (3) reduce horizontal unignited jet flammability hazard distances. For the 1-wall vertical barrier and 3-wall barrier configurations the simulations of the peak overpressure hazard from ignition were found to be approximately 40kPa on the release side of the barrier while (approximately 5-3 kPa) on downstream side of the barrier.

5. Acknowledgements

This work was supported by the U.S. Department of Energy, Office of Energy Efficiency and Renewable Energy, Hydrogen, Fuel Cells and Infrastructure Technologies Program under the Codes and Standards subprogram element managed by Antonio Ruiz.

6. References

American Institute of Chemical Engineers, Guidelines for Evaluating the Characteristics of Vapor Cloud Explosions, Flash Fires, and BLEVEs, Center for Chemical Process Safety of AICHE, 3 Park Ave., New York, NY, 1994.

Barlow, R. S. and Carter, C. D., Raman/Rayleigh/LIF Measurements of Nitric Oxide Formation in Turbulent Hydrogen Jet Flames, *Combustion and Flame*, Vol. 97, 261-280, 1994.

Birch, A.D., Brown, D.R., Dodson, M.G., Swaffield, F., The Structure and Concentration Decay of High Pressure Jets of Natural Gas, Combustion Science and Technology, Vol. 36, 249-261, 1984.

Burns, S. P., SYRINX – User's Manual, unpublished Sandia National Laboratories Report, August 5, 1999.

Coward, H.F, and Jones, G.W., "Limits of Flammability of Gases and Vapors," Bureau of Mines Bulletin 503, 1952.

Houf, W.G., and Schefer, R.W., "Predicting Radiative Heat Fluxes and Flammability Envelopes from Unintended Releases of Hydrogen," Int. Jour. of Hydrogen Energy, Vol. 32, 136-151, January 2007.

FLACS Version 8 Users Guide, GEXCON, Bergen, Norway, 2003.

Houf, W. G., Evans, G, and Schefer, R. W., "Analysis of Jet Flames and Unignited Jets from Unintended Releases of Hydrogen", 2nd International Conference on Hydrogen Safety, San Sebastian, Spain, September 11-13, 2007.

2006 International Fire Code, International Code Council, Inc., 2006.

Leckner, B., Spectral and Total Emissivity of Water Vapor and Carbon Dioxide, *Combustion and Flame*, Vol. **19**, 33-48, 1972.

Magnussen, B. F., Modelling of NO_x and Soot Formation by the Eddy Dissipation Concept, Int. Flame Research Foundation 1st Topical Orientation Meeting, Amsterdam, 1989.

Moen, C.D., Evans, G.H., Domino, S.P. and Burns, S.P., A Multi-Mechanics Approach to Computational Heat Transfer, proceedings 2002 ASME Int. Mech. Eng. Congress and Exhibition, New Orleans, IMECE2002-33098, Nov. 17-22, 2002.

NFPA 68 Standard on Explosion Protection by Deflagration Venting, National Fire Protection Association, Dec. 20, 2006.

Papageorgakis, G. C. and Assanis, D. N., Comparison of Linear and Nonlinear RNG-based k-ε Models for Incompressible Turbulent Flows, Num. Heat Transfer, Part B, Vol. 35, 1-22, 1999.

Schefer, R.W., Houf, W.G., Williams, T.C., Bourne, B., and Colton, J., "Characterization of High-Pressure, Under-Expanded Hydrogen-Jet Flames," International Journal of Hydrogen Energy, Vol. 32, 2081–2093, August, 2007.

Schefer, R.W., Houf, W.G., Bourne, B., and Colton, J., "Spatial and Radiative Properties of an Open-Flame Hydrogen Plume," International Journal of Hydrogen Energy, Vol. 31, 1332-1340, August 2006.

Schneider, G.E., Elliptic Systems: Finite-Element Method 1, Handbook of Numerical Heat Transfer (Minkowycz, W. J., Sparrow, E.M., Schneider, G.E. and Pletcher, R.H. Eds.), J. Wiley & Sons, Inc., New York, Ch. 10, 379-420, 1988.

Shapiro, A. H., The Dynamics and Thermodynamics of Compressible Fluid Flow – Vol. 1, The Ronald Press Co., New York, 116-118, 1953.

Shirvill, L.C. and Roberts, T.A., Designing for Safe Operations: Understanding the Hazards Posed by High Pressure Leaks from Hydrogen Refuelling Stations, USA National Hydrogen Association Annual Conference, March 12-16, 2006, Long Beach, CA, USA.

Tanaka, T., Azuma, T., Evans, J.A., Cronon, P.M., Johnson, D.M. and Cleaver, R.P., Experimental Study on Hydrogen Explosions in a Full-Scale Hydrogen Filling Station, HYSAFE ICHS International Conference on Hydrogen Safety, Paper 120036, Pisa, Italy, September 8-10, 2005.

Tchouvelev, A.V., Cheng, Z, Agranat, V.M. and Zhubrin, S.V., Effectiveness of Small Barriers as Means to Reduce Clearance Distances, Int. Jour. of Hydrogen Energy, Vol. 32, 1409-1415, 2007.

Thurgood, C.P., Pollard, A., and Becker, H.A., "The T_N Quadrature Set for the Discrete Ordinates Method," J. Heat Transfer, Vol. 117, 1068-1070, Nov. 1995.

Winters, W. S. and Evans, G. H., Final Report for the ASC Gas-Powder Two-Phase Flow Modelling Project AD2006-09, Sandia National Laboratories Report No. SAND2006-7579.

Zebetakis, M.G., U.S. Bureau of Mines, Bulletin 627, 1965.